Spaces of anthropogenic CO_2 emissions compatible with climate boundaries

Thomas Bossy[1,2], Philippe Ciais[1], Katsumasa Tanaka[1,3], Franck Lecocq[4], Philippe Bousquet[1], Thomas Gasser[1,2]*

[1]Laboratoire des sciences du climat et de l'environnement (LSCE), IPSL, CEA/CNRS/UVSQ, Université Paris-Saclay, 91191 Gif-sur-Yvette, France

[2]International Institute for Applied System Analysis (IIASA), 2361 Laxenburg, Austria

[3]Earth System Division, National Institute for Environmental Studies (NIES), Tsukuba, 305-8506, Japan

[4] Centre International de Recherche sur l'Environnement et le Développement (CIRED), CNRS, EHESS, AgroParisTech, PontsParisTech, CIRAD, 94736 Nogent-sur-Marne, France

*Corresponding author: gasser@iiasa.ac.at

Final published article:

Bossy, T., Ciais, P., Tanaka, K., Lecocq, F., Bousquet, P., & Gasser, T. (2025). Spaces of anthropogenic CO2 emissions compatible with climate boundaries. *Nature Climate Change* 10.1038/s41558-025-02460-5.

Abstract

Climate boundaries are planetary boundaries for the climate system: limits within which humanity can sustainably prosper. Here, we introduce a new modelling framework to analyse global warming, ocean acidification, sea level rise, and Arctic sea ice melt. Using a reduced-form model, we map out anthropogenic CO_2 emissions, carbon dioxide removal (CDR), and solar radiation management (SRM) pathways compatible with these boundaries. We define safety levels as the probability to stay within one or several boundaries considering physical uncertainty. If CO_2 emissions peak in 2030, net-zero CO_2 is reached in 2050, CDR capacity is 10 PgC per year, and without SRM, remaining within the global warming boundary of 2°C exhibits a safety level of 80%. When all four boundaries are considered together, the safety level drops to 35%. Our results highlight key trade-offs in mitigation options and suggest a need to assess climate boundaries holistically to develop sustainable future strategies.

Planetary boundaries define a safe operating space within which humanity can develop and prosper[1,2]. Staying within boundaries implies limiting the level of anthropogenic interference with the Earth system[3]. Therefore, there is a space of anthropogenic interference, and notably CO_2 emissions, compatible with every planetary boundary and any combination thereof[4]. This compatible space has been explored for individual planetary boundaries, for instance limiting phosphorus or nitrogen fertilizers inputs[5–7], or for the global warming boundary of 2°C[8–10]. Some interactions between few planetary boundaries have been explored[3,4,11,12] but a systematic exploration of the compatible space constrained by multiple boundaries is lacking.

Here, we introduce a modelling framework to systematically explore the compatible space for four climate boundaries: global warming (GW), ocean acidification (OA), rate of sea level rise (RSLR) and Arctic sea ice (ASI) melt. These boundaries differ from the original planetary boundaries of Rockstrom et al.[1]. They were chosen for modelling purposes, as a more direct quantification of physical impacts of climate change, and to give a complementary insight to the rich planetary boundary literature. For these boundaries – individually or as a constellation – we investigate the shape of the compatible space of CO2 emissions using indicators of these emissions describing the limits beyond which a boundary is breached (for a certain safety level).

A typical indicator found throughout the literature to characterize the space compatible with the global warming boundary is the remaining carbon budget[10]: the total amount of CO_2 that can be emitted before reaching a given global warming level. This concept is based on the near-linear relationship[13] between cumulative anthropogenic CO_2 emissions and global warming. However, the carbon budget provides a limited description of the compatible space of anthropogenic interference, and the near-linear relationship tends to break down for other boundaries such as sea level rise (SLR)[14].

Here, to characterize compatible spaces under multiple boundaries, we focus on four indicators: the year of peak CO_2 emissions, the year of net-zero CO_2 emissions, the maximum annual amount of Carbon Dioxide Removal (CDR), and the maximum annual amount of Solar Radiation Management (SRM) if applicable. Those four characteristics allow us to summarize a wide range of mitigation strategies.

Space of emissions constrained by climate boundaries

To derive the compatible space of emissions, we propose a inverse (or backward) approach[15] using the Pathfinder carbon-climate model. Pathfinder is a reduced-complexity model calibrated through Bayesian inference on state-of-the-art complex Earth system models and constrained using observational and IPCC AR6 data[16]. A large set of atmospheric CO_2 concentration and global temperature time series until year 2500 are generated randomly and used as input (Methods). We then back-calculate compatible CO_2 emissions through mass balance, given the simulated land and ocean carbon sinks, including permafrost emissions. The non-CO_2 radiative forcing is further obtained by inversion of the model's energy balance equations. We estimate CDR and SRM as subcomponents of net CO_2 emissions and non-CO_2 radiative forcing, respectively, using a mitigation floor[17] taken from the most intensive mitigation trajectories of the AR6 scenarios database[18], and assuming that mitigation beyond that floor is attributable to CDR for CO_2 emissions and to SRM for non-CO_2 radiative forcing (Methods). Pathfinder emulates physical variables related to our climate boundaries (Methods). To account for the Earth system's physical uncertainty, the model is run under 1500 different configurations obtained after the Bayesian calibration (Methods). The combination of configurations and pathways gives several million possible futures used to map the compatible spaces.

The temperature pathways we generate all stay below +2°C and asymptotically reach +1.5°C, and by construction remain within the GW boundary[1,19]. The three additional boundaries are: avoiding a collapse of ASI in summer, which is equivalent to not exceeding 1.7 ± 0.2°C of global warming[20]; avoiding OA with a pH decrease limited to -0.2 unit compared to the preindustrial level, a threshold beyond which oceanic biodiversity integrity may be threatened[21–23]; and remaining below 5 cm of SLR per decade, a precautionary threshold consistent with previous studies[22,23].

Because our framework accounts for physical uncertainty (Box and Figure 1), we define the concept of safety level as the fraction of the 1500 configurations where we find at least one emission pathway compatible with the targeted climate boundaries, in a space of emissions that can also be bounded by constraints on the four key characteristics introduced earlier. We can explicit the definition as

$$\text{safety level} = \; n_{\text{config}}(\textit{boundary, CDR, SRM, peak year, net zero year}) / \, N_{\text{config}}$$

Where N_{config} = 1500 is the total number of configurations and n_{config} is the number of configurations with at least one pathway compatible with the considered boundary and under the chosen conditions on pathways characteristics (CDR, SRM, peak year, net-zero year). Therefore, a 100% safety level guarantees that it is physically possible to not exceed the boundary whereas a safety level of 0% means that it is impossible to remain within the considered climate boundary. We discuss more stringent definitions of the safety level in Supplementary Information.

To map a compatible space, we determine the limit value of a pathway's characteristic beyond which a climate boundary is breached for a given safety level. For instance, if in 67% of the model's configurations at least one pathway remains below 2°C with CO_2 emissions peaking in 2031, and this condition is not met with CO_2 emissions peaking in 2032 or later, then 2031 marks the limit for peak CO_2 emissions to meet the GW boundary with a 67% safety level. Note that the pathways found to be compatible with a given boundary are not necessarily the same across physical configurations (Box and Methods). Therefore, we actually map the point of the compatible space beyond which the climate boundaries are breached (with a certain probability). Our safety level differs from the IPCC's definition of confidence level[24], as the latter assesses the chances for one scenario to cross boundaries while the former is the probability that among all scenarios at least one remains within the boundaries.

Spaces of emissions compatible with climate boundaries

First, we confirm that our ensemble of compatible emission trajectories encompasses all IPCC AR6 scenarios[16] that keep temperature below 2°C (Supplementary Figure 1). This implies that our approach explores a larger space of possibilities than existing AR6 scenarios.

We find that without any CDR, it is possible to respect the GW boundary with a safety level of only 11%, even if CO_2 emissions peak in 2025. the corresponding safety levels are 10% for RSLR, 10% for OA, 5% for ASI, and 4% for all four boundaries combined (Figure 2). In contrast, if large amounts of CDR are available (up to 10 PgC yr^{-1}), the safety level for GW increases to 80% with a peak in 2030 and net zero later than 2050, and is 78% for RSLR, 71% for OA, 37% for ASI, and 35% for all boundaries combined (Figure 2). This indicates that the restriction of the compatible space is non-linear when combining boundaries. The gap in safety levels between no-CDR scenarios with early peak emissions and CDR scenarios with late peak emissions highlights the fact that CDR essentially enables delaying the peak of emissions, which we investigate next.

The trade-offs between the year of peak emission and the amount of available CDR for a 67% safety level is shown in Figure 3 (also Extended Data Figure 1a). The slope of the frontier in Figure 3a quantifies the deployment of (maximum annual) CDR required to compensate a delay in the peak date of CO2 emissions. For example, peaking at the earliest year requires less than 4 PgC yr^{-1} of CDR, while peaking in 2030 requires more than 8 PgC yr^{-1} of CDR to stay under the GW boundary. Over a range of peak dates going from 2023 to 2030, the compatible space for RSLR and OA is approximately the same as for GW. The ASI boundary, however, requires a stricter compatible space and necessitates at least 5.2 PgC yr^{-1} of CDR with the earliest peak or the assumed maximum value of 10 PgC yr^{-1} with a peak in 2027, because this boundary embeds additional physical uncertainty in its definition. Even for this maximum level of CDR, the ultimate dates for emissions to peak is 2026 to remain within all boundaries, 2027 for ASI, 2030 for OA, and 2031 for RSLR and GW (for a 67% safety level).

While a delay in the peak of CO_2 emissions can be compensated to some extent by the deployment of CDR, this deployment does not need to happen in the very short term. Even for the ambitious target of keeping within all boundaries with a 67% safety level, CDR does not appear at significant levels (defined as >0.5 PgC yr^{-1}) before 2045 (Extended Data Figure 1b). To respect the GW boundary alone (at a 67% safety level), CDR does not need to be significantly deployed before 2060, as long as CO_2 emissions peak before 2030.

Achieving net-zero later than 2050 is mainly incompatible with climate boundaries in the case of a late peak of emissions (Figure 2). For instance, staying within the OA boundary with a CO_2 emission peak in 2030 and up to 10 PgC yr^{-1} of CDR has a 87% safety level if net zero is reached before 2050 (Figure 2), which drops to 71% if net-zero is reached later than that. Similar drops are observed for GW (90% to 80%), ASI (55% to 37%), RSLR (89% to 78%) and all boundaries together (55% to 35%). The drop in the safety level due to a late net-zero date is significantly larger for a peak in 2030 than for a peak in 2023, which demonstrates that reaching net-zero earlier helps offset a late peak in emissions.

The trade-off between net-zero year and peak emissions for all boundaries at the 67% safety level is shown in Figure 3b. With the earliest peak, net-zero does not have to be reached before 2080 to remain within the OA or the RSLR boundary as also shown in Figure 2. However, remaining within the ASI boundary requires net-zero to occur no later than 2060. Delaying the peak of emissions requires net-zero CO_2 emissions to occur earlier in the second half of the 21st century. A late peak means more emissions to compensate for and less time to do so. For the RSLR boundary, we find pathways that peak in 2031 if net-zero is reached in 2055, whereas if net-zero is reached in 2079, emissions must peak by 2025 at the latest. This example shows a stronger effect of short-term action on long-term strategy: delaying the peak by 6 years requires bringing net-zero forward by 24 years.

The trade-off between peak emissions and the maximum rate of CDR deployment at the 67% safety level is displayed in Figure 4a. With a maximum rate of -0.5 PgC yr^{-2}, it is already too late to remain within the ASI boundary, and remaining within other boundaries requires a peak at the latest in 2027 for OA, in 2028 for RSLR and in 2029 for GW. Increasing the rate of CDR deployment (up to -1.5 PgC yr^{-2})

would allow to delay the emissions peak by a few years (2027 for ASI, 2030 for OA, and 2031 for RSLR and GW).

Adding solar geoengineering to the compatible space

Considering solar geoengineering to mitigate climate change raises ethical questions as this technology has potential unexpected consequences[25]. We nevertheless investigate whether SRM (represented as additional negative non-CO2 radiative forcing) extends the compatible space of emissions.

Allowing the use of SRM in addition to CDR improves the safety level of the compatible spaces for a late peak in CO_2 emissions. With SRM, the safety level is 63% for an emissions peak in 2035 when respecting all boundaries, compared to 1% without SRM (Figure 2). Specifically, there is a near-linear trade-off between postponing the year of peak CO_2 emissions and implementing SRM (Figure 4b) for all boundaries except OA. We see that allowing up to 2 W m^{-2} of SRM only permits delaying peak emissions by 6 years (2036 instead of 2030) to stay within the OA boundary with a safety level of 67%, because SRM does not reduce atmospheric CO2 concentration. This minimal benefit may be over-optimistic because our OA quantification neglects the effects of temperature and of sulphur deposition from SRM itself.

Our approach also allows to quantify SRM as a substitute for CDR in the case of a late peak in emissions. If the peak is later than 2030, SRM could work as a substitute for CDR: at a 67% safety level. There is a substitution of approximatively 2 PgC yr^{-1} of CDR per 0.25 W m^{-2} of SRM allowed, to stay within any individual or combined boundary (Extended Data Figure 2). Contrarily to the trade-off between SRM and the year of peak CO_2, this trade-off is also valid for the OA boundary, because in this study CDR is mainly used to decrease atmospheric CO_2 and the substitution would occur after its peak, that is when SRM does not threaten the pH threshold of the OA boundary.

Strengths and limitations of the approach

This study shows that there is a very low probability of meeting climate boundaries without CDR, even if CO_2 emissions peak in 2025. Significant CDR implementation may allow for a later emissions peak, but the trade-off is limited and peaking later than 2030 still jeopardizes the chances to remain within climate boundaries. Our results also suggest that ambitious CDR need not be deployed before the second half of the 21st century and that early net-zero emissions (between 2050 and 2060) can offset later peaks, contrasting with typical results arguing for net-zero emissions in 2050. In addition, the inclusion of SRM can improve safety levels, except for the OA boundary due its being impacted by atmospheric CO_2 concentration. Those conclusions are the consequences of our approach that ignores socio-economic constraints. This choice allows us to explore the widest space of possible scenarios unburdened by paradigmatic choices such as cost-optimality[26–28]. The compatible spaces we explore can be further reduced by applying socio-economic criteria to eliminate scenarios that are deemed irrelevant or unrealistic.

Our results show that assumptions about the level of future CDR and SRM have a significant impact on the space of anthropogenic activities compatible with climate boundaries, in line with previous studies[17,29–31]. Our inverse approach requires defining CDR and SRM as the additional mitigation needed when a floor of positive emissions or radiative forcing is reached. Because this floor is the lower bound of the AR6 scenarios envelope[18] (excluding these technologies), we implicitly assume that all possible mitigation efforts have been made before resorting to CDR or SRM. This assumption implies that our results are conservative: if conventional mitigation cannot deliver as in the AR6 scenarios, the need for CDR or SRM will be larger than presented here. Similarly, we impose a limit on the rate of CDR deployment that is based on the fastest decarbonization rate in AR6 scenarios (approximately -1.5 PgC yr^{-2}). The sensibility of our results (notably the peaking date) to this assumption is illustrated in Figure 4b. This constraint is fairly permissive and strengthening it would significantly reduce the compatible spaces, forcing all pathways to peak almost immediately.

Our treatment of non-CO_2 radiative forcing must be understood with all its limitations. Non-CO_2 GHGs and aerosols have opposite radiative effects. While we distinguished both when defining the non-CO2 mitigation floor (Methods), attributing further radiative forcing decrease to SRM alone is simplistic. Unfortunately, splitting the non-CO2 component is not feasible with our inverse modelling approach, as explicitly modelling the related biogeochemical cycles would significantly increase computing cost, and maintaining inverse solvation of the system would reduce the comprehensiveness of the explored compatible space. Similarly, we did not include the impact of sulphate emissions for SRM on OA[32–34], noting that our results would not be significantly modified (Supplementary Information) because most pathways with SRM are already excluded from the space compatible with the OA boundary (Figure 4b), and additional acidification would only reinforce this incompatibility. Overall, we recognize that future developments of the model should prioritize the improvement of the non-CO_2 term with a particular focus on the correlation between methane and aerosols forcings.

With our notion of safety level, we assess the existence of at least one emission pathway compatible with one or more climate boundaries, in a space bounded by constraints on the emission pathways' key characteristics. Importantly, in a given physical configuration of the model, not all pathways with a key characteristic equal to the limit value of the compatible space adhere to the climate boundary. Indeed, the chosen characteristics are relevant proxies, but they must be combined to comprehensively describe the limits of the actual compatible space. In other words, individual limits quantified in this work are necessary but not sufficient conditions to stay within climate boundaries, unless enough of them are combined to form a comprehensive description of the compatible space. Furthermore, we investigated safer constraints requiring more than one emissions pathway to be compatible with the boundaries, which leads to more stringent limits of the compatible space (Supplementary Figures 2 and 3 Supplementary Text).

Global warming primarily depends on cumulative CO_2 emissions rather than on the magnitude or timing of the emission peak[35], so that long-term mitigation strategies often prioritize achieving a net-zero CO_2 emissions target[36]. However, the diversification of boundaries diminishes the relevance of the carbon budget as a unique indicator to define compatible spaces of emissions[10]. We showed here that carbon budgets fail to capture the tightening of the compatible space, the uselessness of SRM against ocean acidification, or the importance of the timing of emission peak. Our study highlights the importance of considering additional key mitigation characteristics to comprehensively map the compatible space of future CO_2 emissions. In particular, the timing of peak CO_2 emissions emerges as a key factor in trade-off mechanisms. We have quantified how an earlier emissions peak can enable a shift in the net-zero CO_2 date, reduce the need for CDR measures, and eliminate the need for SRM techniques.

Our concept of compatible space resembles the tolerable window approach introduced in the early 2000s[22,37–39] and extends the notion of the "closing door" introduced by Stocker[40]. In addition, the narrowing of the compatible space caused by combining climate boundaries has been shown by Steinacher et al.[41]. However, our study goes beyond their 55 scenarios and the remaining carbon budget as the sole characterisation of anthropogenic pathways. Our four climate boundaries could be supplemented by additional boundaries arising from physical or anthropogenic impacts of climate change, up to considering all planetary boundaries. The selected thresholds are also subject to debate due to the inherent uncertainties and judgement values associated with this choice[2,42].

The trade-off between peak emissions and negative emissions has already been highlighted in the results of projections based on integrated assessment models (IAM), but the AR6 scenario framework[18] explored a narrower range of pathways than our study, often with strong negative emissions in the second half of the 21st century[30,43], without inclusion of SRM, and limited to the 2100 horizon. Here, we produced a large ensemble of pathways ex-ante, ignoring socio-economic and technological constraints, which allowed us to search for original scenarios consistent with the Paris Agreement that were not analysed by IAMs. Pathfinder covers a wider range of possible pathways than was explored by the IAMs (Supplementary Figure 1). Although the IAMs propose scenarios that respect all climate boundaries, they are based primarily on the GW boundary and do not explore all alternatives.

Our inverse approach implicitly considers all cases of zero emission commitment (ZEC)[44], which is the committed temperature change after reaching net-zero CO2 emissions. Indeed, Pathfinder exhibits a range of ZEC that covers the positive and negative domains, as complex models do[16]. Since we use an asymptotic definition for the long-term temperature target in our pathways, a positive ZEC implies maintaining negative emissions to compensate for this committed warming, whereas a negative ZEC leads to (slightly) positive emissions of CO2 while global temperature stabilises. In the latter case, since we explore physical feasibility, configurations with negative ZEC would simply respect the targeted boundaries more easily, thereby contributing to raising the safety level, because it is defined as the percentage of configurations that match all the selected constraints.

The non-linearity of boundary combinations argues for diversification of climate impact indicators to be considered ex-ante by scenario developers. It is instructive and complementary to IAMs to expand the scope of emissions compatible with these boundaries. Even if these pathways turn out not to be economically optimal, it is critical to first draw what is physically possible and then decide what is socio-economically feasible and acceptable. To assess the relevance of a pathway in the socio-economic dimension, coupling of Pathfinder with an IAM or simple impact models seems a natural next step in our work[28], as it would enable the exploration of compatible spaces that are also constrained in the socio-economic and technological dimensions. In summary, the framework developed in this study can contribute to enhancing dialogue among the Earth system, impacts, and IAM communities, and encourage scenario narratives that explore a wider range of possible futures in an integrated manner.

Box 1: Method to determine compatible spaces

Our inverse approach is illustrated step by step in Figure 1. First, we generate around 15,000 different trajectories of global mean surface temperature and atmospheric CO2 concentration that follow historical data and, for temperature, asymptotically reach 1.5°C with an overshoot of up to the 2°C global warming level (Methods). Those trajectories are used as inputs to Pathfinder (step 1).

To account for physical uncertainties, we run the model (step 2) with 1500 sets of parameters that can be seen as 1500 possible states of the world with their own physics, all independent and calibrated on historical observations. The parameters of the input trajectories (step 1) are chosen independently in every physical configuration.

All pathways stay below the +2°C GW boundary by construction, and we define permissive conditions on CO_2 anthropogenic emissions and non-CO_2 radiative forcing to remain within reasonable ranges: in step 3, we exclude pathways rising too quickly (quicker than the most pessimistic pathway from AR6 scenarios), using too much CDR (more than 10 PgC yr^{-1}), or seeing too fast decarbonization (faster than the fastest decarbonization rate in the AR6 scenarios). In Figure 1, we use the envelope of all the pathways that stay within a given boundary to illustrate the compatible space. We compare the envelope of the space compatible with the GW boundary (black envelope in Figure 1) with envelopes obtained for other climate boundaries, either independently (green envelope for OA) or combined (purple envelope). As explained in the main text, respecting more boundaries leads to narrower envelopes.

The next steps are illustrated with the OA boundary only in Figure 1. To express the compatible space in terms of key characteristics, we search for limit values on combinations of these pathway characteristics for which there remains one last pathway in the compatible space. In step 4, we extract three of these final pathways corresponding to a specific combination of date of emission peak and CDR deployed. It shows that delaying the CO_2 emissions peak requires more CDR deployment.

In step 5, we represent the compatible space of two characteristics: CDR deployment and CO_2 emission peak, for the OA boundary. Inside this compatible space, the model always finds at least one pathway. The limit of the domain gives the trade-off between the two pathway characteristics that are represented, assuming conditions on other key characteristics remain unchanged.

These successive steps are illustrated for one Pathfinder configuration only in Figure 1, but they are repeated for all 1500 configurations. Therefore, for a given set of conditions on pathway characteristics and climate boundaries, we assess the existence of at least one compatible pathway in all individual physical states of the world (i.e. configurations). We define the safety level as the percentage of configurations that find at least one emissions pathway compatible with one or more climate boundaries, for the chosen set of conditions on pathway characteristics. This ultimate pathway may be different across configurations.

Acknowledgments

T.G. acknowledges support from the European Union's Horizon 2020 and Horizon Europe research and innovation programmes under grant agreements no. 820829 (CONSTRAIN), 951542 (GENIE), 101003536 (ESM2025) and. 101056939 (RESCUE).

Author Contributions Statement

T.G. designed the research following a discussion with F.L.; T.B. performed the research and wrote the original draft; T.B., P.C., K.T., F.L., P.B. and T.G. discussed the research and edited the manuscript.

Competing interests

The authors declare no competing interests.

Figure 1. Overview of the inverse framework applied in this study. Here, only one of the 1500 configurations of Pathfinder is shown for illustrative purpose; we reiterate this process with all configurations to take physical uncertainty into account. We define the safety level as the percentage of configurations that find at least one emissions pathway compatible with one or more climate boundaries for a given set of conditions on pathway characteristics. See Box text for a detailed step-by-step walkthrough.

Figure 2. Safety levels of compatible spaces defined by various combinations of conditions on pathway characteristics. Panels a) to f) distinguish conditions on the date of CO_2 emissions peak and of net-zero. *Net-zero after 2050* means that CO_2 net-zero is reached in 2050 or later. No information on net-zero means that this pathways characteristic is not constrained. *Peak in 2023, 2025, 2030 and 2035* means that the compatible CO_2 pathways reach their peak in 2023, 2025, 2030, or 2035. Markers distinguish conditions on speculative technologies (CDR and SRM), *Up to 10 PgC yr^{-1} of CDR available* assumes that only CDR will be available, possibly up to 10 PgC yr^{-1}. *Without CDR and SRM* assumes that neither SRM nor CDR will be available. *CDR available and SRM allowed* assumes SRM being possibly used up to 2 W m^{-2} in addition to up to 10 PgC yr^{-1} of CDR available. Finally, the *No CDR available but up to 2W m^{-2} of SRM allowed* case assumes that CDR will never be available, but SRM can be used up to 2 W m^{-2}. Marker lines show the 90%, 67% and 50% safety levels.

Figure 3. Trade-offs between pathway characteristics at the 67% safety level. Panel a) shows compatible spaces depending on CDR availability (PgC yr^{-1}) and the year of CO_2 emissions peak. Panel b) shows compatible spaces depending on the years of CO_2 emissions net-zero and peak. Shaded areas represent the spaces compatible with climate boundaries and their combination. Plain lines give the frontier of the compatible space: farther right or above these lines, it is not possible to stay within the boundary. Markers plots show the limit of the compatible space if the other pathway characteristic is not constrained and for three safety levels: 50% (squares), 67% (diamonds) and 90% (circles). Black is for the GW boundary, green for the OA boundary, red for the RSLR boundary, blue for the ASI boundary, and purple for the combination of all boundaries. Reading example with black dashed lines on panel a): If up to 6 PgC yr^{-1} of CDR are available, all boundaries (and the ASI boundary) can be respected with a peak in 2024, the OA boundary with a peak in 2028 and the RSLR and GW boundaries with a peak in 2029, with a 67% safety level (i.e. in 67% of the states of the world).

Figure 4. Trade-offs between pathway characteristics at the 67% safety level. Panel a) displays the trade-off between the year of CO2 emissions peak and the maximum rate of CDR deployment (PgC yr^{-2}). Panel b) displays the trade-off between the year of CO_2 emissions peak and the amount of SRM (W m^{-2}) allowed. Shaded areas represent the spaces compatible with one climate boundary. Plain lines give the frontier of the compatible space. Black is for the GW boundary, green for the OA boundary, red for the RSLR boundary, blue for the ASI boundary, and purple for the combination all boundaries.

References

1. Rockström, J. *et al.* Planetary Boundaries: Exploring the Safe Operating Space for Humanity. *Ecol. Soc.* **14**, art32 (2009).
2. Steffen, W. *et al.* Planetary boundaries: Guiding human development on a changing planet. *Science* **347**, 1259855 (2015).
3. Richardson, K. *et al.* Earth beyond six of nine planetary boundaries. *Sci. Adv.* **9**, eadh2458 (2023).
4. Lade, S. J. *et al.* Human impacts on planetary boundaries amplified by Earth system interactions. *Nat. Sustain.* **3**, 119–128 (2019).
5. Schulte-Uebbing, L. F., Beusen, A. H. W., Bouwman, A. F. & De Vries, W. From planetary to regional boundaries for agricultural nitrogen pollution. *Nature* **610**, 507–512 (2022).
6. Bouwman, L. *et al.* Exploring global changes in nitrogen and phosphorus cycles in agriculture induced by livestock production over the 1900–2050 period. *Proc. Natl. Acad. Sci.* **110**, 20882–20887 (2013).
7. Mekonnen, M. M. & Hoekstra, A. Y. Global Anthropogenic Phosphorus Loads to Freshwater and Associated Grey Water Footprints and Water Pollution Levels: A High-Resolution Global Study. *Water Resour. Res.* **54**, 345–358 (2018).
8. Rogelj, J. *et al.* Scenarios towards limiting global mean temperature increase below 1.5 °C. *Nat. Clim. Change* **8**, 325–332 (2018).
9. Rogelj, J. *et al.* A new scenario logic for the Paris Agreement long-term temperature goal. *Nature* **573**, 357–363 (2019).
10. Lamboll, R. D. *et al.* Assessing the size and uncertainty of remaining carbon budgets. *Nat. Clim. Change* **13**, 1360–1367 (2023).
11. Lade, S. J., Fetzer, I., Cornell, S. E. & Crona, B. A prototype Earth system impact metric that accounts for cross-scale interactions. *Environ. Res. Lett.* **16**, 115005 (2021).
12. Chrysafi, A. *et al.* Quantifying Earth system interactions for sustainable food production via expert elicitation. *Nat. Sustain.* **5**, 830–842 (2022).
13. Intergovernmental Panel On Climate Change (Ipcc). *Climate Change 2021 – The Physical Science Basis: Working Group I Contribution to the Sixth Assessment Report of the Intergovernmental Panel on Climate Change.* (Cambridge University Press, 2023). doi:10.1017/9781009157896.
14. Mengel, M. *et al.* Future sea level rise constrained by observations and long-term commitment. *Proc. Natl. Acad. Sci.* **113**, 2597–2602 (2016).
15. Pfleiderer, P. *et al.* Reversal of the impact chain for actionable climate information. *Nat. Geosci.* (2025) doi:https://doi.org/10.1038/s41561-024-01597-w.
16. Bossy, T., Gasser, T. & Ciais, P. Pathfinder v1.0.1: a Bayesian-inferred simple carbon–climate model to explore climate change scenarios. *Geosci. Model Dev.* **15**, 8831–8868 (2022).
19. Ipcc. *Global Warming of 1.5°C: IPCC Special Report on Impacts of Global Warming of 1.5°C above Pre-Industrial Levels in Context of Strengthening Response to Climate Change, Sustainable Development, and Efforts to Eradicate Poverty.* (Cambridge University Press, 2022). doi:10.1017/9781009157940.
20. Niederdrenk, A. L. & Notz, D. Arctic Sea Ice in a 1.5°C Warmer World. *Geophys. Res. Lett.* **45**, 1963–1971 (2018).
21. Gattuso, J.-P. *et al.* Contrasting futures for ocean and society from different anthropogenic CO_2 emissions scenarios. *Science* **349**, aac4722 (2015).
22. Kvale, K. *et al.* Carbon Dioxide Emission Pathways Avoiding Dangerous Ocean Impacts. *Weather Clim. Soc.* **4**, 212–229 (2012).
23. Schubert, R. *et al. The Future Oceans - Warming Up, Rising High, Turning Sour.* (2006).
24. Mastrandrea, M. D. *et al.* The IPCC AR5 guidance note on consistent treatment of uncertainties: a common approach across the working groups. *Clim. Change* **108**, 675–691 (2011).
25. Babiker, M. *et al.* Cross-sectoral Perspectives.
26. Grubb, M., Wieners, C. & Yang, P. Modeling myths: On DICE and dynamic realism in integrated assessment models of climate change mitigation. *WIREs Clim. Change* **12**, (2021).

27. Pindyck, R. S. The Use and Misuse of Models for Climate Policy. *Rev. Environ. Econ. Policy* **11**, 100–114 (2017).
28. Bossy, T. *et al.* Least-cost and 2 °C-compliant mitigation pathways robust to physical uncertainty, economic paradigms, and intergenerational cost distribution. *Environ. Res. Clim.* **3**, 025005 (2024).
29. Tokarska, K. B. & Zickfeld, K. The effectiveness of net negative carbon dioxide emissions in reversing anthropogenic climate change. *Environ. Res. Lett.* **10**, 094013 (2015).
30. Obersteiner, M. *et al.* How to spend a dwindling greenhouse gas budget. *Nat. Clim. Change* **8**, 7–10 (2018).
31. Aengenheyster, M., Feng, Q. Y., Van Der Ploeg, F. & Dijkstra, H. A. The point of no return for climate action: effects of climate uncertainty and risk tolerance. *Earth Syst. Dyn.* **9**, 1085–1095 (2018).
32. Duarte, C. M. *et al.* Is Ocean Acidification an Open-Ocean Syndrome? Understanding Anthropogenic Impacts on Seawater pH. *Estuaries Coasts* **36**, 221–236 (2013).
33. Doney, S. C. *et al.* Impact of anthropogenic atmospheric nitrogen and sulfur deposition on ocean acidification and the inorganic carbon system. *Proc. Natl. Acad. Sci.* **104**, 14580–14585 (2007).
34. Visioni, D., Pitari, G. & Aquila, V. Sulfate geoengineering: a review of the factors controlling the needed injection of sulfur dioxide. *Atmospheric Chem. Phys.* **17**, 3879–3889 (2017).
35. Allen, M. R. *et al.* Warming caused by cumulative carbon emissions towards the trillionth tonne. *Nature* **458**, 1163–1166 (2009).
36. Van Soest, H. L., Den Elzen, M. G. J. & Van Vuuren, D. P. Net-zero emission targets for major emitting countries consistent with the Paris Agreement. *Nat. Commun.* **12**, 2140 (2021).
37. Bruckner, T., Hooss, G., Füssel, H.-M. & Hasselmann, K. Climate System Modeling in the Framework of the Tolerable Windows Approach: The ICLIPS Climate Model. (2003).
38. Petschel-Held, G., Schellnhuber, H.-J., Bruckner, T., Tóth, F. L. & Hasselmann, K. The Tolerable Windows Approach: Theoretical and Methodological Foundations. (1999).
39. Zickfeld, K. & Bruckner, T. Reducing the risk of Atlantic thermohaline circulation collapse: sensitivity analysis of emissions corridors. *Clim. Change* **91**, 291–315 (2008).
40. Stocker, T. F. The Closing Door of Climate Targets. *Science* **339**, 280–282 (2013).
41. Steinacher, M., Joos, F. & Stocker, T. F. Allowable carbon emissions lowered by multiple climate targets. *Nature* **499**, 197–201 (2013).
42. Rockström, J. *et al.* Safe and just Earth system boundaries. *Nature* (2023) doi:10.1038/s41586-023-06083-8.
43. Riahi, K. *et al.* The Shared Socioeconomic Pathways and their energy, land use, and greenhouse gas emissions implications: An overview. *Glob. Environ. Change* **42**, 153–168 (2017).
44. MacDougall, A. H. *et al.* Is there warming in the pipeline? A multi-model analysis of the Zero Emissions Commitment from CO_2. *Biogeosciences* **17**, 2987–3016 (2020).

Methods

The Pathfinder model

It is a compilation of existing formulations that describe parts of the Earth system, chosen for their good balance between mathematical simplicity and physical accuracy, and brought together to form a consistent carbon-climate model of reduced complexity. Here, the global temperature anomaly (*T*) and global atmospheric CO_2 concentration (*C*) are given as independent inputs to the model. The model has 77 parameters. 33 of them are fixed and the other 44 parameters constrained through a Bayesian calibration[45] based on observations and AR6 assessments, as detailed in a previous paper[16]. The drivers (*T* and *C*) are updated to observations available until 2021. However, the model is not designed to provide insights for 2022, the first year of the simulation, due to the functional form used to generate scenarios. We thus show and discuss the results only from 2023 onward.

A comprehensive description of Pathfinder is provided in Bossy et al.[16], and briefly summarized here. The climate subcomponent that links *T* to effective radiative forcing (*R*) follows a widely used 2-box model with deep ocean heat uptake efficacy[46]. The total *R* is caused by atmospheric CO_2 (following the IPCC AR5 logarithmic formula[47]) and an aggregate of non-CO_2 species. Anthropogenic CO_2 emissions are determined by the balance between atmospheric CO_2, ocean and land carbon sinks, and permafrost carbon emissions. The ocean carbon cycle follows the structure of the Bern Simple Climate Model[48]. The land carbon cycle follows the formulation of the compact Earth system model OSCAR[49], although it is aggregated into one global biome, land cover change is ignored, and it accounts for the so-called passive soil carbon that is ignored in most complex models[50]. It leads to a total of four land carbon pools. Emissions from permafrost thaw are calculated with the emulator developed by Gasser et al.[51], but aggregated into one unique region. Sea level rise is split into thermosteric, glaciers, Greenland and Antarctica effects that each follows a first-order differential equation[14,52]. Additionally, ocean surface acidification follows a polynomial fit on *C*[53].

The use of Bayesian inference allows for the integration of observational data into simplified models like Pathfinder[45]. This approach involves deriving joint probability distributions of parameters based on prior knowledge of those distributions and the distributions of observed variables in the model. The posterior probability of a sample from the joint parameter distribution, given a set of observations, is proportional to the likelihood of the model simulating the observations and the prior probability of the parameters. The 44 Pathfinder parameters estimated using Bayesian inference are constrained using a set of 19 observations pertaining to most aspects of the global Earth System[16]: *T* (present-day value and derivative across five datasets[54–58]), ocean heat content[59], non-CO_2 radiative forcing[47], recent global carbon budget[60] (for land, ocean, and atmosphere), preindustrial carbon pools[61] (land and atmosphere), and satellite-derived sea level rise speeds[62]. The prior distributions of the parameters are determined based on literature values and multi-model ensembles. To estimate the posterior distributions, a full-rank Automatic Differentiation Variational Inference (ADVI) algorithm is used[63], and the Pathfinder model is solved using an explicit Eulerian exponential integrator scheme. The paper by Bossy et al.[16], provides detailed information on the parameter and observational constraints, as well as diagnostic tests that validate the model.

Input trajectories

We randomly and independently draw temperature and atmospheric CO_2 concentration trajectories using four different approaches grouped into "series" (Supplementary Figures 4 and 5 for illustration). Series 1, 2 and 3 correspond to different analytical expressions while series 4 is derived from AR6 scenarios[18]. All series are divided in sub-series, and they all have common constraints:

(1) $T, \frac{d}{dt}T$ and C are defined and differentiable;

(2) We impose an upper boundary so that $T \leq 2°C$;

(3) We also impose $\lim_{t\to\infty} T = 1.5°C$;

(4) We randomly choose an asymptotic value for C which is determined by the share $k_{x,final}$ of non-CO_2 components in the global radiative forcing. $k_{x,final}$ is uniformly drawn from one of three equiprobable ensembles: $k_{x,final} \in]-1;-0.1[$; $k_{x,final} \in [-0.1;0.1]$; $k_{x,final} \in]0.1;0.66[$

In Series 1, for X being T or C, we choose X of the form $X(t) = X_0 + (X_{lim} - X_0)\cdot\omega(t-t_0) + \alpha\cdot t\cdot(1-\omega(t-t_0))$, with $X_0 = X(t=t_0)$ the initial value of X given by the historical calibration, with t_0=2021, and X_{lim} the asymptotic value. We determine α so that $\left.\frac{dX}{dt}\right|_{t=t_0} = \left.\frac{dX}{dt}\right|_0$, where $\left.\frac{dX}{dt}\right|_0$ is the differentiated variable given by the historical calibration in 2021.

$\omega(t)$ is the function we use to distinguish the sub-series. This function must tend towards 0 for $t = 0$ and towards 1 for $t \to \infty$. To keep the continuity and differentiability for X and $\frac{dX}{dt}$, ω must be continuously differentiable at least once. In series 1a, $\omega(t) = 1 - e^{-\mu_0 t - \mu_1^2 t^2}$ [64], in series 1b, $\omega(t) = \frac{t}{t+\mu_1 e^{-\mu_0 t}}$, and in series 1c, $\omega(t) = \frac{\mu_0 t^2 + \mu_1 t}{1+\mu_0 t^2}$. Parameter distributions are given in Supplementary Table 1.

Series 2 follows the probability density function of a Kumaraswamy distribution[65] until it peaks (i.e. for $t < t_{peak}$), $X(t < t_{peak}) = X_0 + [X_{peak} - X_0]\cdot[1-(1-(\tau_o/(\tau_o - t_{peak}))^{\alpha})^{-\beta}\cdot(1-((\tau_o - t)/(\tau_o - t_{peak}))^{\alpha})^{\beta}]$. Peaking dates ($t_{peak}$) and peaking values ($X_{peak}$) are chosen randomly in ensembles that are compatible with our constraints and for which we can maintain continuity and differentiability of X and $\frac{dX}{dt}$. τ_o is defined such as $f(\tau_o) = -t_{peak}$ with $f(t) = -t\cdot((1-\frac{t_{peak}}{t})^{\alpha} - 1) - \alpha\cdot\beta\cdot\frac{X_{peak}-X_0}{\left.\frac{dX}{dt}\right|_0}$. Sub-series have different functional forms after the peak ($t > t_{peak}$) to converge to the asymptotic value X_{lim}. Series 2a follows the probability density function of a normal distribution such as $X(t \geq t_{peak}) = X_{lim} + (X_{peak} - X_{lim})\cdot e^{-\frac{(t-t_{peak})^2}{\tau^2}}$. With $\tau = \frac{\sqrt{X_{peak}-X_{lim}}}{\sqrt{X_{peak}-X_0}}\cdot(t_{peak}-\tau_o)\cdot\left(1-\left(-\frac{\tau_o}{t_{peak}-\tau_o}\right)^{\alpha}\right)^{\beta/2}\cdot\sqrt{\frac{2}{\alpha^2\cdot\beta\cdot(\beta-1)}}$. Series 2b follows the probability function of a log-normal distribution so $X(t \geq t_{peak}) = X_{lim} + (X_{peak} - X_{lim})\cdot e^{-0.5\frac{\log(t/t_{peak})^2}{\sigma^2}}$.

With $\sigma = \frac{\sqrt{X_{peak} - X_{lim}}}{\sqrt{X_{peak} - X_0}} \cdot \left(1 - \frac{\tau_o}{t_{peak}}\right) \cdot \left(1 - \left(-\frac{\tau_o}{t_{peak} - \tau_o}\right)^{\alpha}\right)^{\beta/2} \cdot \sqrt{\frac{2}{\alpha^2 \cdot \beta \cdot (\beta - 1)}}$. Series 2c follows the probability function of a Gompertz distribution[66]: $X(t \geq t_{peak}) = X_{lim} + (X_{peak} - X_{lim}) \cdot \eta^{1-t/t_{peak}}\, e^{1-\eta^{1-t/t_{peak}}}$. With $\eta = exp\left(\frac{\sqrt{X_{peak} - X_{lim}}}{\sqrt{X_{peak} - X_0}} \cdot \left(1 - \frac{\tau_o}{t_{peak}}\right) \cdot \left(1 - \left(-\frac{\tau_o}{t_{peak} - \tau_o}\right)^{\alpha}\right)^{-\beta/2} \cdot \sqrt{\frac{2}{\alpha^2 \cdot \beta \cdot (\beta - 1)}}\right)$. We apply all three sub-series to the temperature but only series 2a and 2c to the atmospheric CO_2 concentration. Parameter distributions are given in Supplementary Table 1.

Series 3 follows the solution of the differential system of a damped harmonic oscillator with non-zero initial positions and velocities. Depending on sub-series, it is either in a critical regime (series 3a) under the form $X(t) = X_{lim} + \left(X_0 - X_{lim} + \left(\kappa \cdot (X_0 - X_{lim}) + \left.\frac{dX}{dt}\right|_0\right) \cdot t\right) \cdot e^{-\kappa t}$, or in an over-critical regime (aperiodic) for series 3b, $X(t) = X_{lim} + \left[(X_0 - X_{lim}) \cdot cosh(\sqrt{\kappa^2 - \Omega^2} \cdot t) + \frac{\kappa \cdot (X_0 - X_{lim}) + \left.\frac{dX}{dt}\right|_0}{\sqrt{\kappa^2 - \Omega^2}} \cdot sinh(\sqrt{\kappa^2 - \Omega^2} \cdot t)\right] \cdot e^{-\kappa t}$. Parameter distributions are given in Supplementary Table 1.

Series 4 is derived from the AR6 scenarios. Initially, we simulate all AR6 scenarios[22] using Pathfinder (as detailed in the subsequent section), and select only those scenarios where the maximum temperature remains below 2°C. These *T* and *C* time series are the first members of Series 4. However to add more scenarios "inspired" by AR6 scenarios, we introduce noise generated through an AR(1) process[67]. We then apply an 11-year moving average to smoothen the trajectories affected by noise. We infer the lost 11 values by following the trend observed in the original T or C time series. To ensure the generated pathways are continuously differentiable, we fit the resulting trajectories with spline functions. These functions are defined piecewise by polynomials and allow for differentiation. Similar to other series, we impose constraints on the initial values of *X* and $\frac{dX}{dt}$ to maintain continuity with the historical trajectory. Additionally, to prevent splines with excessively steep or rapid trends in 2100, we also constrain the derivative at that point with the original value of the AR6 scenario before the noise.

Since Series 4 is derived from AR6 scenarios, the processed trajectories are limited to the year 2100. However, for our purposes, we require pathways that span up to 2500. To address this, we employ the analytical form of Series 3a to extend the trajectories from 2100 to 2500, ensuring continuity and differentiability are maintained throughout the extended period.

Overall, all four series depend on parameters that are chosen independently in every configuration. It means that the set of trajectories is different and independent from one configuration to another.

Implementation of AR6 scenarios in Pathfinder

The AR6 database[23] hosts the results of all scenarios explored by different IAMs assessed by the working group 3 of the IPCC. However, these projections are inconsistent with the historical values of Pathfinder, making it infeasible to directly incorporate the raw data into our model.

In the AR6 database, the drivers are CO_2 emissions and non-CO_2 radiative forcing (R_x). To utilize harmonized and vetted CO_2 emissions and R_x scenarios as inputs in the forward mode of Pathfinder, we perform linear interpolation to convert the decadal data into annual data. Subsequently, we rescale both drivers to align with the historical trajectories of Pathfinder. Due to the inherent natural variability present in Pathfinder's historical runs, it is not possible to directly utilize the year 2021 as a reference for rescaling.

Therefore, we rescale future CO_2 emissions based on the 11-year mean values calculated in Pathfinder's historical and centered in 2016 and we infer the 2021 value using the trend in observational values[60]. This approach ensures consistency with Pathfinder's configurations, as the 11-year mean value is specific to each configuration. The rescaling factor is determined by comparing the reconstructed value for 2021 with the corresponding value in the AR6 scenario.

Similarly, for R_x, we reconstruct the historical value in 2021 by extending the 11-year mean values calculated in Pathfinder's historical trend centred in 2016. Between 2016 and 2021 we incorporate the trend in observational values (based on observations until 2019[29]). However, the treatment of R_x differs from that of CO_2 emissions due to its nature as a radiative forcing resulting from a combination of various GHGs (positive) and aerosols (mostly negative). Consequently, depending on the model's parameterization, the reconstructed historical R_x value in 2021 can be either negative or positive. Rescaling R_x without accounting for this decomposition could potentially lead to an artificial reversal of the sign of R_x in the scenarios. To address this, we decompose R_x and rescale each component separately: $R_x^{AR6} = R_{x,ghgs}^{AR6} + R_{x,aerosols}^{AR6}$, where R_x^{AR6} is the radiative forcing due to non-CO_2 forcers in AR6 scenarios, $R_{x,ghgs}^{AR6}$ is the radiative forcing due to a combination of different GHGs in AR6 scenarios, and $\mathrm{R}_{\mathrm{x,aerosols}}^{\mathrm{AR6}}$ is the radiative forcing due to aerosols in AR6 scenarios. As Pathfinder lacks such a decomposition, we use the IPCC AR6 extrapolated value of $R_{x,ghgs}^{hist} = 1.18 \pm 0.14\, W\, m^{-2}$ in 2021[68]. Assuming a normal distribution we randomly draw one value of the GHG component of R_x for each configuration of Pathfinder. Finally, the rescaling factor for GHGs is $\frac{R_{x,ghgs}^{hist}}{R_{x,ghgs}^{AR6,2021}}$, and the rescaling factor for aerosols is $\frac{R_x^{hist} - R_{x,ghgs}^{hist}}{R_{x,aerosols}^{AR6,2021}}$, where R_x^{hist} is the reconstructed historical value in Pathfinder in 2021 and $R_{x,aerosols}^{AR6,2021}$.and $R_{x,ghgs}^{AR6,2021}$ are the respective AR6 radiative forcing due to a combination of aerosols and different GHGs in 2021.

Definition of SRM and CDR variables

Carbon Dioxide Removal (CDR) Because of our inverse modelling approach, we do not know the CDR contribution to the net anthropogenic CO_2 emission pathways (E_{CO2}) we estimate. To do so, we define a time-dependent floor (CDR_{floor}) below which we consider that CDR is needed (Supplementary Figure 6). This CDR_{floor} follows the lower bound of the CO_2 emission pathways envelope from the AR6 scenarios[23], excluding bio-energy with carbon capture and storage ($E_{CO2,min}^{AR6}$) and CDR from land use harmonized and estimated by Gidden et al.[69]. We consider only vetted scenarios excluding the GCAM 5.3 model scenarios following linear decarbonation until different net-zero dates (from 2035 to 2050)[70]. We add a final filter to exclude scenarios that show net negative emissions despite removing the CDR contribution. We interpret these net negative emissions as a misfiling of CDR and therefore the scenario as not reliable.

In addition, the AR6 scenarios were rescaled to be consistent with both Pathfinder historical values and latest observed trends. Because, in that case, we want CDR to be 0 in 2021, we must rescale $E_{CO2,min}^{AR6}$. This gives:

$$CDR = \begin{cases} E_{CO2} - CDR_{floor} \ if \ E_{CO2} < CDR_{floor} \\ 0 \ otherwise \end{cases}$$

with

$$CDR_{floor} = \frac{E_{CO2,2021}}{E_{CO2,min,2021}^{AR6}} E_{CO2,min}^{AR6},$$

where $E_{CO2,2021}$ is the Pathfinder's anthropogenic CO_2 emissions in 2021 and $E_{CO2,min,2021}^{AR6}$ is the lower bound of the CO_2 emission pathways envelope from the AR6 scenarios in 2021.

Solar Radiation Management (SRM) AR6 scenarios do not include SRM or any removal technology for GHGs other than CO_2. Thus, we directly extract the R_x variable from the AR6 scenarios implemented in Pathfinder, and we select the lower bound of the pathway's envelope (Supplementary Figure 5). We smooth it out by taking its minimum value over a rolling period of 5 years ($R_{x,min}^{AR6}$). Finally, we offset this already rescaled floor by Pathfinder's 2021 value ($R_{x,2021}$). That is:

$$SRM = \begin{cases} R_x - SRM_{floor} \ if \ R_x < SRM_{floor} \\ 0 \ otherwise \end{cases}$$

with

$$SRM_{floor} = R_{x,2021} - R_{x,min,2021}^{AR6} + R_{x,min}^{AR6},$$

where $R_{x,min,2021}^{AR6}$ is the lower bound of the R_x pathways envelope from the AR6 scenarios in 2021.

Data availability

No raw data is provided with this article because of the total size (>500 GB). However, we provide a code to generate this data.

Code availability

The source code of Pathfinder is openly available at https://github.com/tgasser/Pathfinder (last access: 16 October 2023). A frozen version of the code as developed in the paper can be found on Zenodo at https://doi.org/10.5281/zenodo.7003848 (ref[71]). Additional code and data are available on Zenodo at https://doi.org/10.5281/zenodo.15235819 (ref[72]). This contains the code to reproduce the input trajectories of Pathfinder as well as some examples of post-processing.

References (Methods only)

45. Ricciuto, D. M., Davis, K. J. & Keller, K. A Bayesian calibration of a simple carbon cycle model: The role of observations in estimating and reducing uncertainty. *Glob. Biogeochem. Cycles* **22**, 2006GB002908 (2008).
46. Geoffroy, O. *et al.* Transient Climate Response in a Two-Layer Energy-Balance Model. Part II: Representation of the Efficacy of Deep-Ocean Heat Uptake and Validation for CMIP5 AOGCMs. *J. Clim.* **26**, 1859–1876 (2013).
47. Myhre, G. *et al.* Anthropogenic and Natural Radiative Forcing. in *Climate Change 2013 – The Physical Science Basis* (ed. Intergovernmental Panel On Climate Change) 659–740 (Cambridge University Press, 2014).
48. Strassmann, K. M., Joos, F. & Strassmann, K. The Bern Simple Climate Model (BernSCM) v1.0: an extensible and fully documented open-source re-implementation of the Bern reduced-form model for global carbon cycle–climate simulations. *Geosci Model Dev* (2018).
49. Gasser, T. *et al.* The compact Earth system model OSCAR v2.2: description and first results. *Geosci. Model Dev.* **10**, 271–319 (2017).
50. He, Y. *et al.* Radiocarbon constraints imply reduced carbon uptake by soils during the 21st century. *Science* **353**, 1419–1424 (2016).
51. Gasser, T. *et al.* Path-dependent reductions in CO2 emission budgets caused by permafrost carbon release. *Nat. Geosci.* **11**, 830–835 (2018).
52. Goodwin, P. *et al.* Pathways to 1.5 °C and 2 °C warming based on observational and geological constraints. *Nat. Geosci.* **11**, 102–107 (2018).
53. Bernie, D., Lowe, J., Tyrrell, T. & Legge, O. Influence of mitigation policy on ocean acidification. *Geophys. Res. Lett.* **37**, 2010GL043181 (2010).
54. Cowtan, K. & Way, R. G. Coverage bias in the HadCRUT4 temperature series and its impact on recent temperature trends. *Q. J. R. Meteorol. Soc.* **140**, 1935–1944 (2014).
55. Morice, C. P., Kennedy, J. J., Rayner, N. A. & Jones, P. D. Quantifying uncertainties in global and regional temperature change using an ensemble of observational estimates: The HadCRUT4 data set. *J. Geophys. Res. Atmospheres* **117**, 2011JD017187 (2012).
56. Rohde, R., Muller, R., Jacobsen, R., Perlmutter, S. & Mosher, S. Berkeley Earth Temperature Averaging Process. *Geoinformatics Geostat. Overv.* **01**, (2013).
57. Hansen, J., Ruedy, R., Sato, M. & Lo, K. GLOBAL SURFACE TEMPERATURE CHANGE. *Rev. Geophys.* **48**, RG4004 (2010).
58. Smith, T. M., Reynolds, R. W., Peterson, T. C. & Lawrimore, J. Improvements to NOAA's Historical Merged Land–Ocean Surface Temperature Analysis (1880–2006). *J. Clim.* **21**, 2283–2296 (2008).
59. Detection and Attribution of Climate Change: from Global to Regional. in *Climate Change 2013 – The Physical Science Basis* (ed. Intergovernmental Panel On Climate Change) 867–952 (Cambridge University Press, 2014). doi:10.1017/CBO9781107415324.022.
60. Friedlingstein, P. *et al.* Global Carbon Budget 2023. *Earth Syst. Sci. Data* **15**, 5301–5369 (2023).
61. Ciais, P. *et al.* Carbon and Other Biogeochemical Cycles. in *Climate Change 2013 – The Physical Science Basis* (ed. Intergovernmental Panel On Climate Change) 867–952 (Cambridge University Press, 2014).
62. Church, J. A. *et al.* Sea Level Change. in *Climate Change 2013 – The Physical Science Basis* (ed. Intergovernmental Panel On Climate Change) 1137–1216 (Cambridge University Press, 2014).
63. Kucukelbir, A. Automatic Differentiation Variational Inference. *J. Mach. Learn. Res.* **18**, (2017).
64. Huntingford, C. *et al.* Flexible parameter-sparse global temperature time profiles that stabilise at 1.5 and 2.0 °C. *Earth Syst. Dyn.* **8**, 617–626 (2017).
65. Kumaraswamy, P. A generalized probability density function for double-bounded random processes. *J. Hydrol.* **46**, 79–88 (1980).
66. Gompertz, B. On the nature of the function expressive of the law of human mortality, and on a new mode of determining the value of life contingencies. (1825).

67. Salvatier, J., Wiecki, T. V. & Fonnesbeck, C. Probabilistic programming in Python using PyMC3. *PeerJ Comput. Sci.* **2**, e55 (2016).
68. Intergovernmental Panel On Climate Change. The Earth's Energy Budget, Climate Feedbacks and Climate Sensitivity Supplementary Material. in *Climate Change 2021 – The Physical Science Basis: Working Group I Contribution to the Sixth Assessment Report of the Intergovernmental Panel on Climate Change* (Cambridge University Press, 2023). doi:10.1017/9781009157896.
69. Gidden, M. J. *et al.* Aligning climate scenarios to emissions inventories shifts global benchmarks. *Nature* **624**, 102–108 (2023).
70. Ou, Y. *et al.* Can updated climate pledges limit warming well below 2°C? *Science* **374**, 693–695 (2021).
71. Gasser, T. Pathfinder: v1.0.1. Zenodo (2022). doi:10.5281/zenodo.7003848.
72. Bossy, T. & Gasser, T. Code for "Spaces of anthropogenic CO2 emissions compatible with climate boundaries". Zenodo (2025). doi:10.5281/zenodo.15235819.

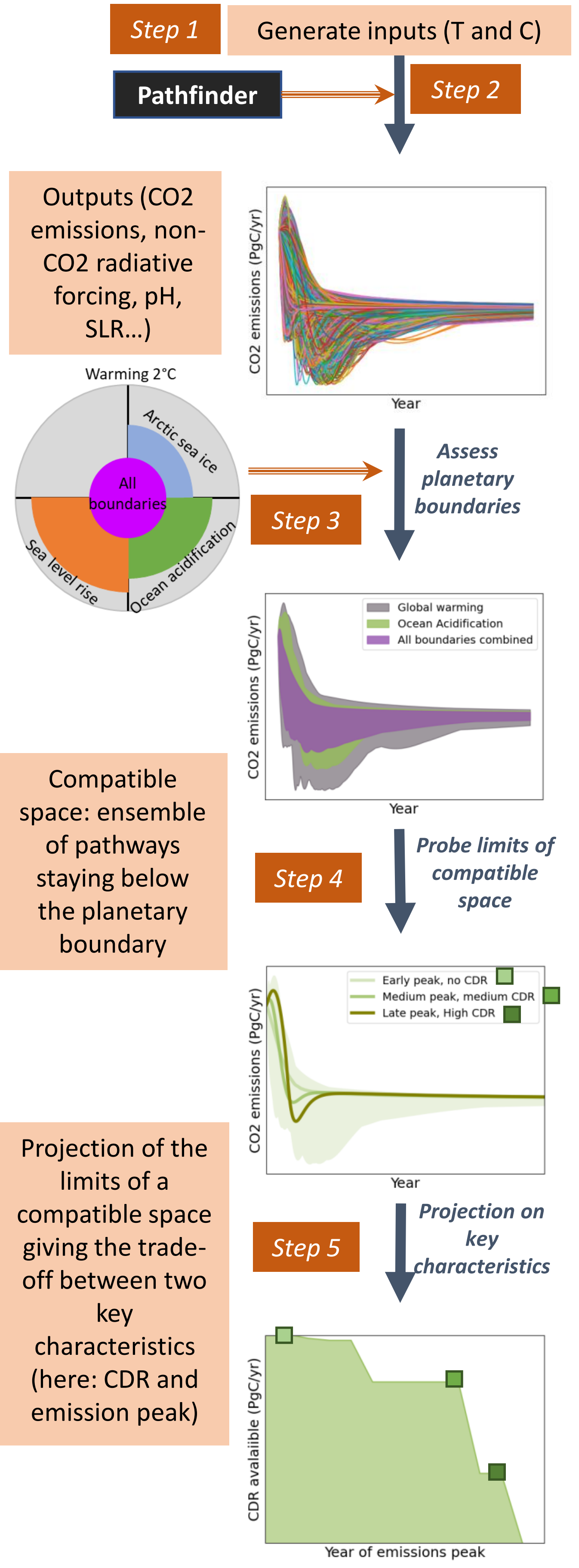

Step 1
Generate inputs (T and C)
Pathfinder
Step 2
Outputs (CO2 emissions, non-CO2 radiative forcing, pH, SLR…)
CO2 emissions (PgC/yr)
Year
Warming 2°C
Arctic sea ice
All boundaries
Sea level rise
Ocean acidification
Step 3
Assess planetary boundaries
Global warming
Ocean Acidification
All boundaries combined
CO2 emissions (PgC/yr)
Year
Compatible space: ensemble of pathways staying below the planetary boundary
Step 4
Probe limits of compatible space
Early peak, no CDR
Medium peak, medium CDR
Late peak, High CDR
CO2 emissions (PgC/yr)
Year
Projection of the limits of a compatible space giving the trade-off between two key characteristics (here: CDR and emission peak)
Step 5
Projection on key characteristics
CDR avalaible (PgC/yr)
Year of emissions peak

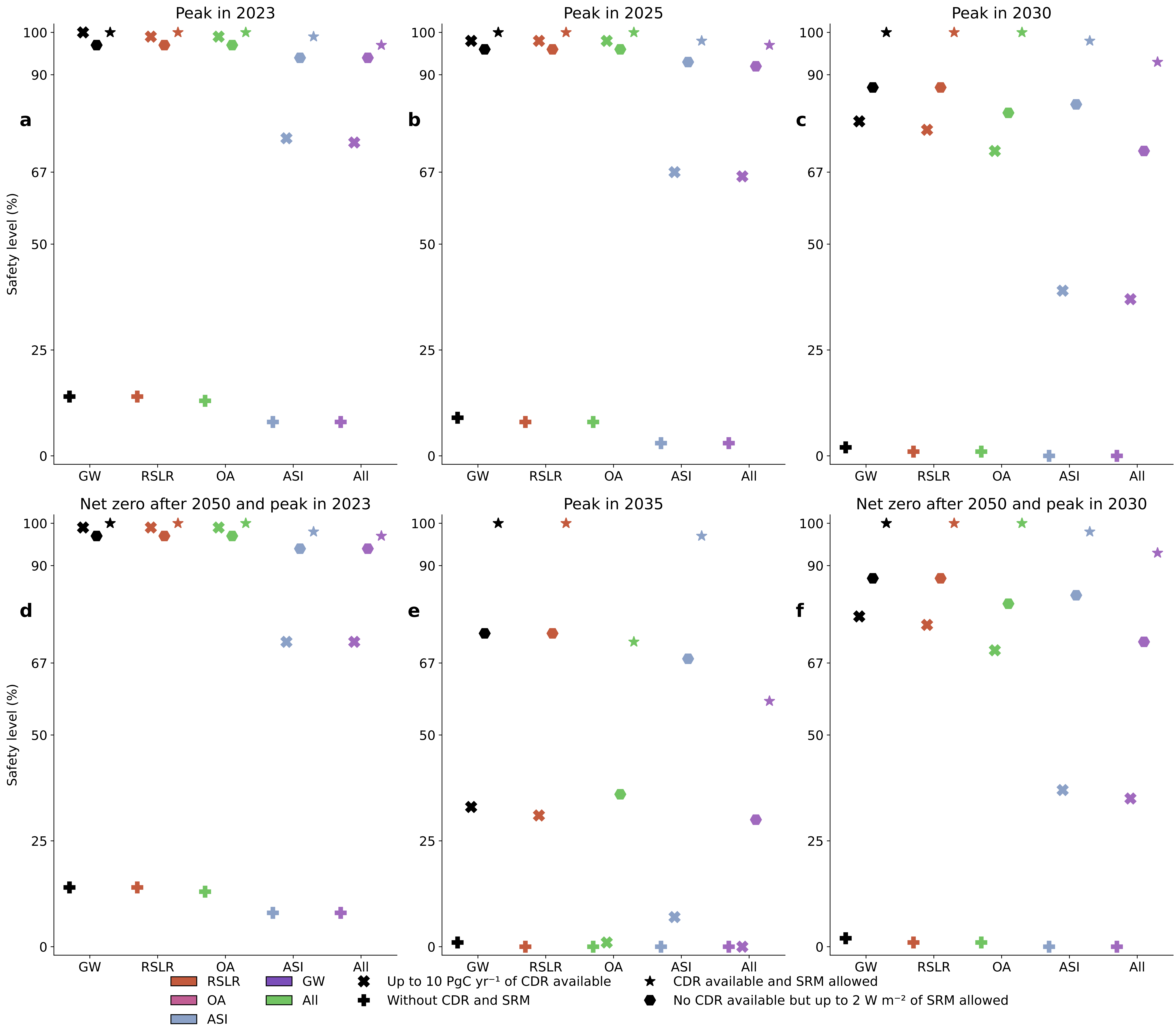
Peak in 2023
Peak in 2025
Peak in 2030
Net zero after 2050 and peak in 2023
Peak in 2035
Net zero after 2050 and peak in 2030
a
b
c
d
e
f
Safety level (%)
100
90
67
50
25
0
GW
RSLR
OA
ASI
All
RSLR
OA
ASI
GW
All
Up to 10 PgC yr⁻¹ of CDR available
Without CDR and SRM
CDR available and SRM allowed
No CDR available but up to 2 W m⁻² of SRM allowed

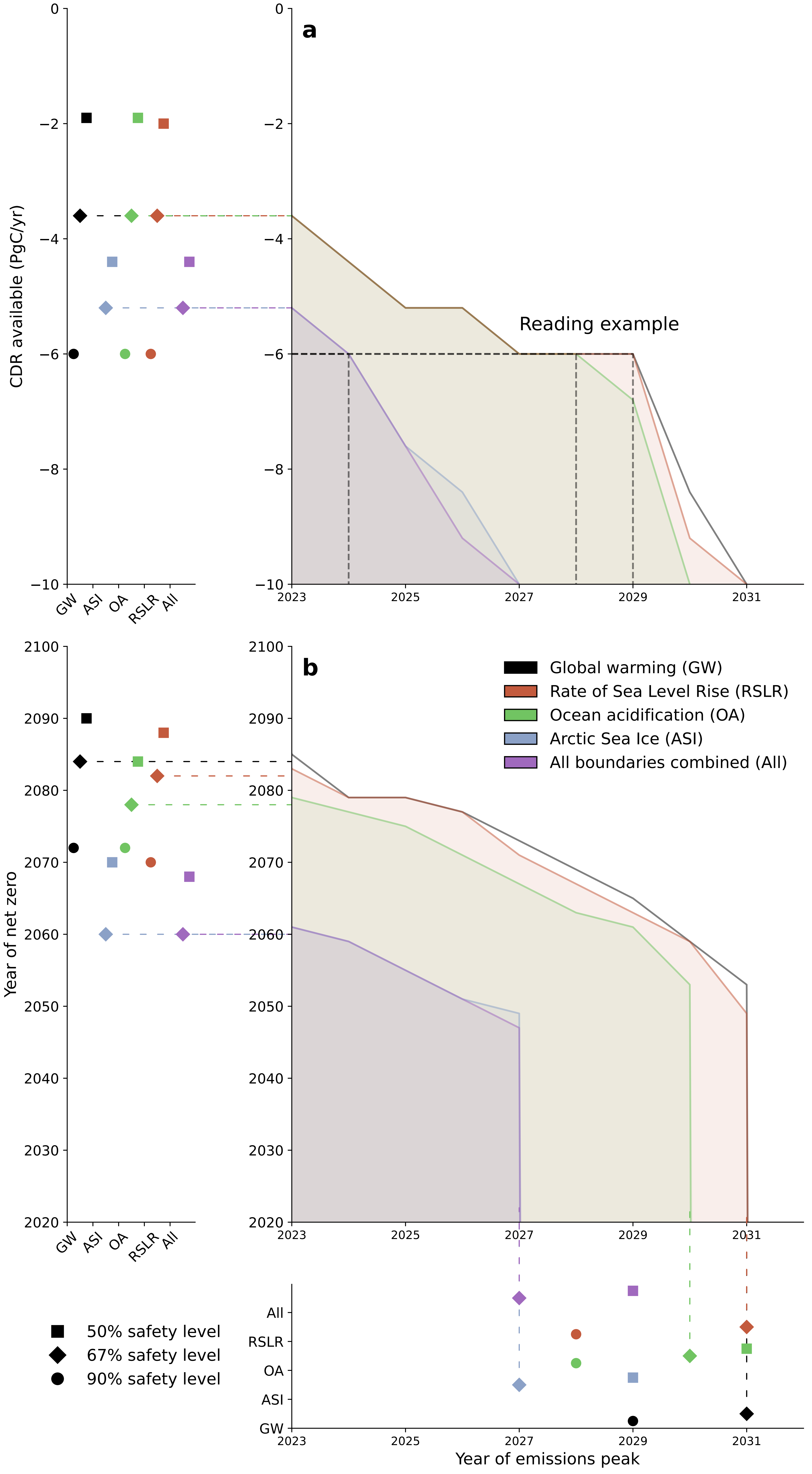

a
b
CDR available (PgC/yr)
Reading example
Year of net zero
Year of emissions peak
GW
ASI
OA
RSLR
All
Global warming (GW)
Rate of Sea Level Rise (RSLR)
Ocean acidification (OA)
Arctic Sea Ice (ASI)
All boundaries combined (All)
50% safety level
67% safety level
90% safety level

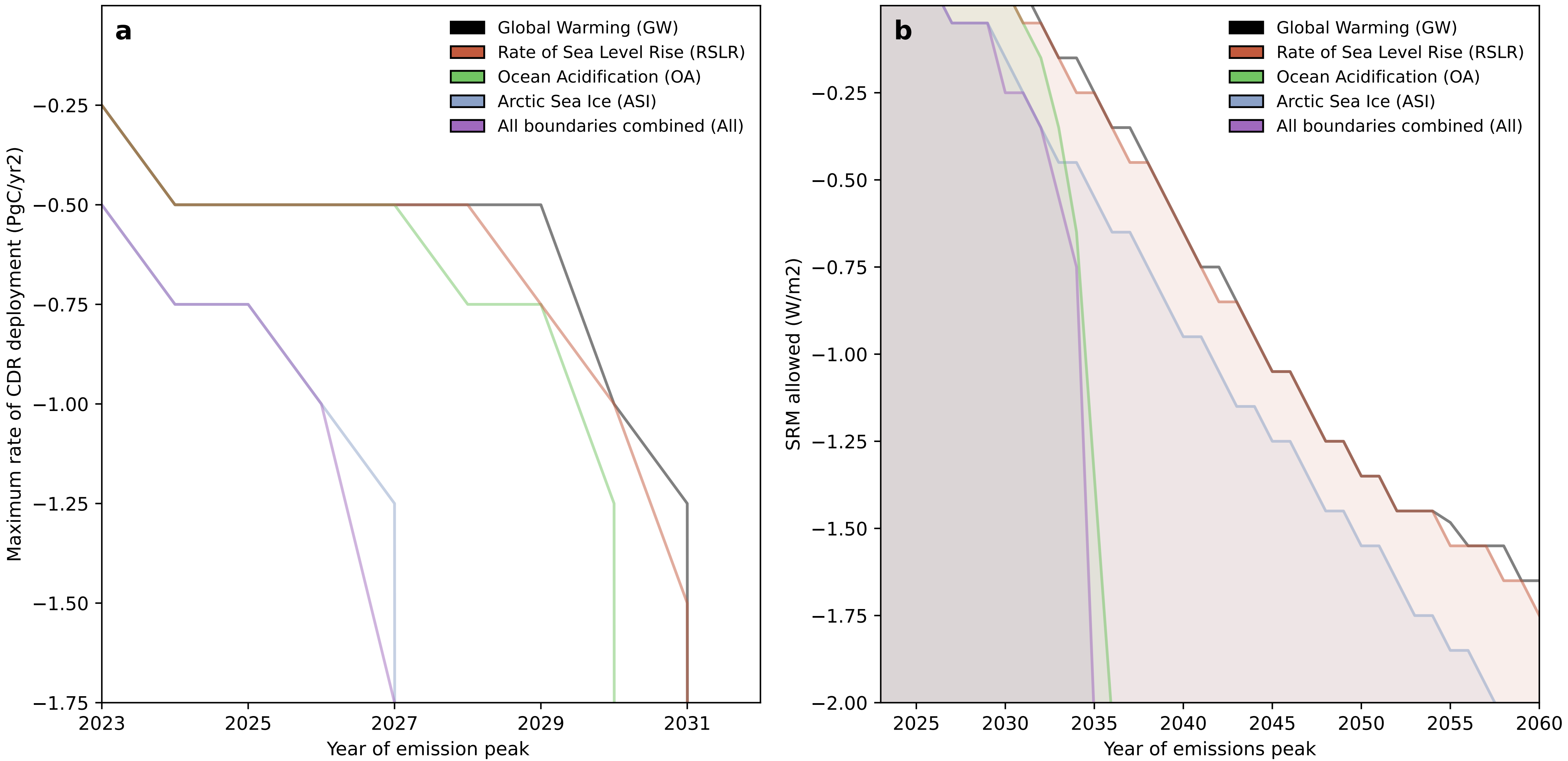
a
Global Warming (GW)
Rate of Sea Level Rise (RSLR)
Ocean Acidification (OA)
Arctic Sea Ice (ASI)
All boundaries combined (All)
Maximum rate of CDR deployment (PgC/yr2)
−0.25
−0.50
−0.75
−1.00
−1.25
−1.50
−1.75
2023
2025
2027
2029
2031
Year of emission peak
b
Global Warming (GW)
Rate of Sea Level Rise (RSLR)
Ocean Acidification (OA)
Arctic Sea Ice (ASI)
All boundaries combined (All)
SRM allowed (W/m2)
−0.25
−0.50
−0.75
−1.00
−1.25
−1.50
−1.75
−2.00
2025
2030
2035
2040
2045
2050
2055
2060
Year of emissions peak

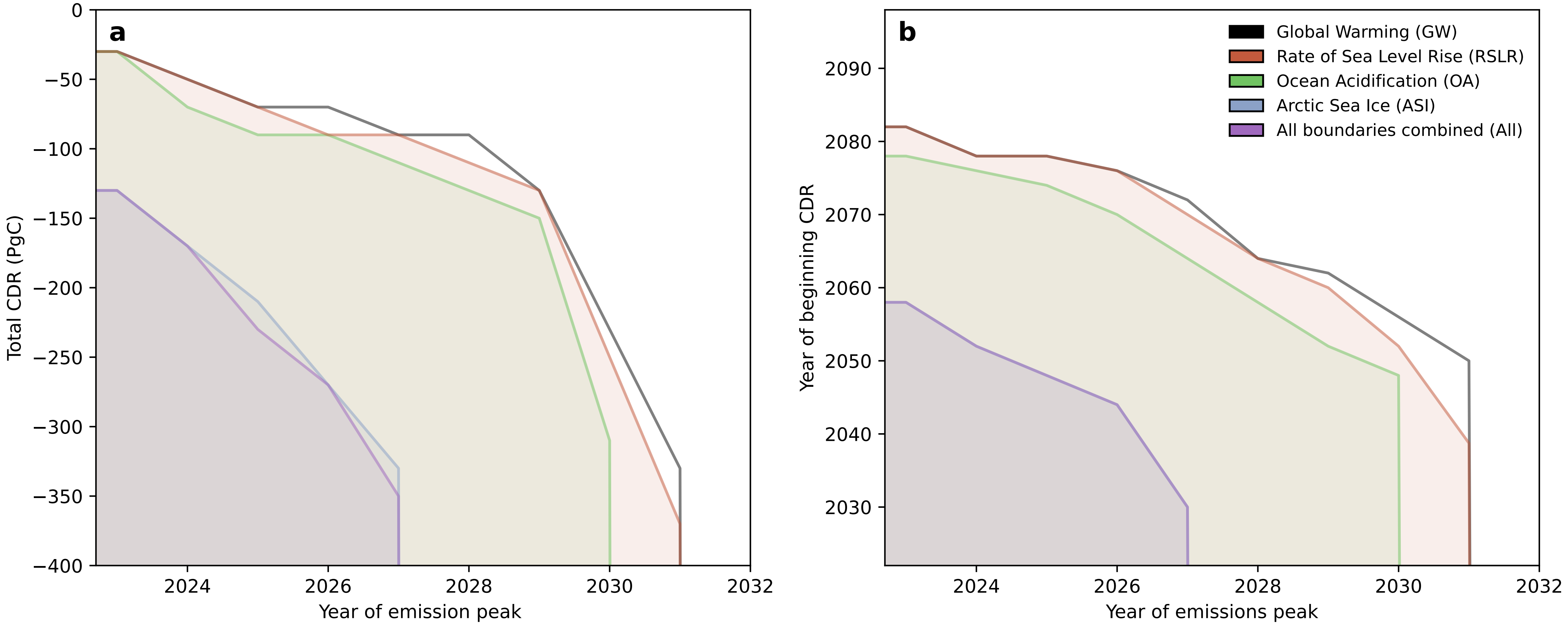
a
0
−50
−100
−150
−200
−250
−300
−350
−400
Total CDR (PgC)
2024
2026
2028
2030
2032
Year of emission peak
b
Global Warming (GW)
Rate of Sea Level Rise (RSLR)
Ocean Acidification (OA)
Arctic Sea Ice (ASI)
All boundaries combined (All)
2090
2080
2070
2060
2050
2040
2030
Year of beginning CDR
2024
2026
2028
2030
2032
Year of emissions peak

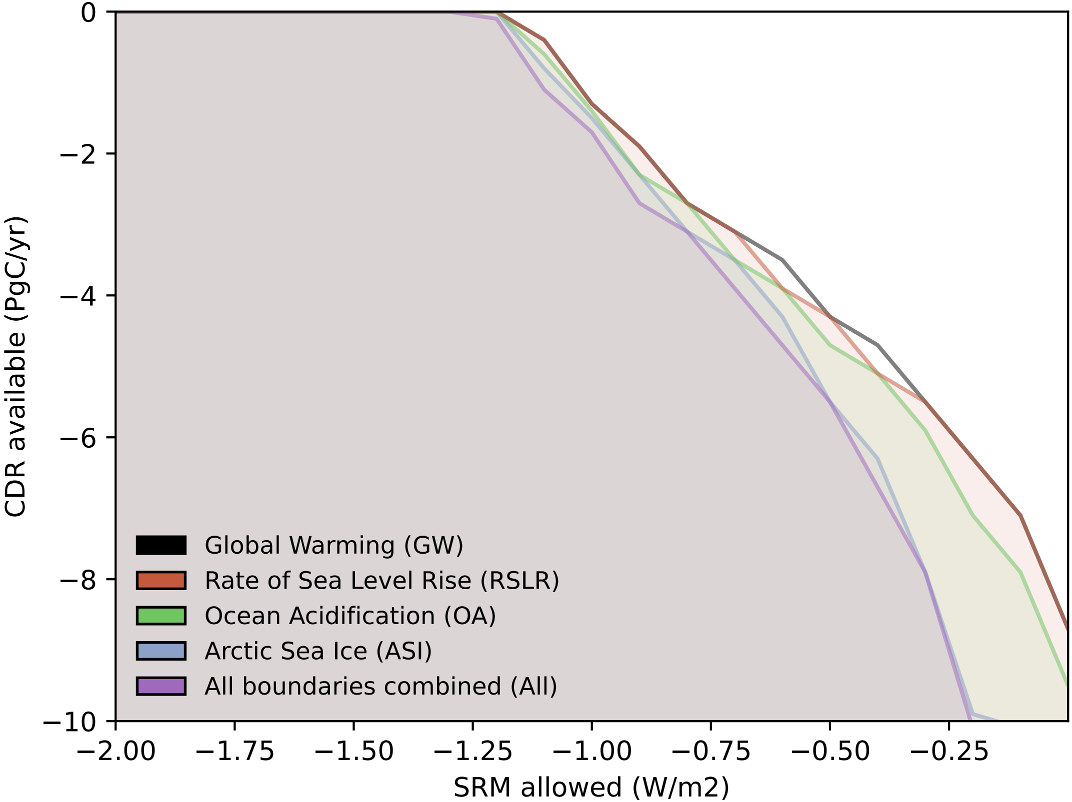

0
−2
−4
−6
−8
−10
CDR available (PgC/yr)
−2.00
−1.75
−1.50
−1.25
−1.00
−0.75
−0.50
−0.25
SRM allowed (W/m2)
Global Warming (GW)
Rate of Sea Level Rise (RSLR)
Ocean Acidification (OA)
Arctic Sea Ice (ASI)
All boundaries combined (All)